Cellular and Molecular Life Sciences (2022) 79:334
https://doi.org/10.1007/s00018-022-04382-3

ORIGINAL ARTICLE

Plant mitochondrial FMT and its mammalian homolog CLUH controls development and behavior in *Arabidopsis* and locomotion in mice

Alexandra Ralevski[1,2] · Federico Apelt[3] · Justyna J. Olas[4] · Bernd Mueller-Roeber[3,4] · Elena I. Rugarli[5,6] · Friedrich Kragler[3] · Tamas L. Horvath[1,2,6,7]

Received: 18 February 2022 / Revised: 15 May 2022 / Accepted: 16 May 2022 / Published online: 2 June 2022

Abstract

Mitochondria in animals are associated with development, as well as physiological and pathological behaviors. Several conserved mitochondrial genes exist between plants and higher eukaryotes. Yet, the similarities in mitochondrial function between plant and animal species is poorly understood. Here, we show that *FMT* (*FRIENDLY MITOCHONDRIA*) from *Arabidopsis thaliana*, a highly conserved homolog of the mammalian *CLUH* (*CLUSTERED MITOCHONDRIA)* gene family encoding mitochondrial proteins associated with developmental alterations and adult physiological and pathological behaviors, affects whole plant morphology and development under both stressed and normal growth conditions. *FMT* was found to regulate mitochondrial morphology and dynamics, germination, and flowering time. It also affects leaf expansion growth, salt stress responses and hyponastic behavior, including changes in speed of hyponastic movements. Strikingly, *Cluh*$^{\pm}$ heterozygous knockout mice also displayed altered locomotive movements, traveling for shorter distances and had slower average and maximum speeds in the open field test. These observations indicate that homologous mitochondrial genes may play similar roles and affect homologous functions in both plants and animals.

Keywords *Arabidopsis thaliana* · Mitochondria · FMT · Hyponasty · Mice · CLUH · Locomotion

Introduction

Mitochondria function is critical for the health and lifespan of an organism, as this organelle regulates vital cellular processes, including metabolism, energy production and apoptosis. Mitochondria can also alter their number, function or morphology in response to various environmental or cellular conditions [7, 32, 49]. Mitochondrial dysfunction due to defects in fission/fusion dynamics, altered trafficking, mutations of mtDNA, or impaired transcription can lead to bioenergetic defects and an overall decline in the fitness of an organism. Dysfunctional mitochondria can induce alterations during development, as well as physiological and pathological malfunctions in adult organisms, for example in various neurodegenerative diseases, including Alzheimer's disease (AD), Parkinson's disease (PD), Huntington's disease (HD) and schizophrenia (SCZ) [4, 5, 21, 22, 24, 25, 36, 38]. Many proteins that regulate these critical mitochondrial processes are highly conserved between species, including plants and animals. Indeed, although plants and animals diverged more than 1.6 billion years ago, numerous human genes, including those known to play a role in disease, have

✉ Tamas L. Horvath
tamas.horvath@yale.edu

1 Department of Comparative Medicine, Yale University School of Medicine, New Haven, CT 06520, USA

2 Yale Center for Molecular and Systems Metabolism, Yale University School of Medicine, New Haven, CT 06520, USA

3 Max Planck Institute of Molecular Plant Physiology, Wissenschaftspark Golm, 14476 Potsdam, Germany

4 Department of Molecular Biology, University of Potsdam, Karl-Liebknecht-Strasse 24-25, 14476 Potsdam, Germany

5 Department of Biology, Institute for Genetics, University of Cologne, Cologne, Germany

6 Institute for Genetics and Cologne Excellence Cluster on Cellular Stress Responses in Aging-Associated Diseases (CECAD), University of Cologne, Cologne, Germany

7 Department of Neuroscience and Kavli Institute for Neuroscience, Yale University School of Medicine, New Haven, CT 06520, USA

conserved orthologs in the plant model organism *Arabidopsis thaliana*. Numerous cellular processes associated with a variety of different diseases, including neurodegenerative disorders such as Parkinson's, Alzheimer's, and Friedrich Ataxia have been elucidated using *Arabidopsis* [6, 19, 29, 52]. Additionally, many discoveries that have increased our understanding of the fundamental mechanisms of disease were either based on previous research in *Arabidopsis* or first elucidated in the plant. These include discoveries in the fields of DNA methylation, innate immunity, protein degradation, ion channels, and many others [53]. Therefore, despite traditionally serving as a model organism for plant biology, there is growing evidence to suggest that research in *Arabidopsis* can play an important role in deepening our understanding of human processes and diseases.

Arabidopsis also contains many conserved orthologs of mitochondrial genes. Similar to animals, plant mitochondria play an important role in development and disease, including stress tolerance and protection from fungal infection [27]. Conserved mitochondrial genes include those that encode the fission proteins fission 1 (FIS1) and dynamin-related protein (DRP) [3, 43, 54, 55], voltage-dependent anion channels (VDACs) [39], the mitochondrial calcium uniporter (MICU) [50] and CLU, a member of the clustered mitochondria superfamily. Initially, CLU was characterized in slime mold (*Dictyostelium discoideum*) [56] and yeast (*Saccharomyces cerevisiae*) [17], deriving its name from the striking phenotype of mitochondrial clustering following a gene knockout (KO), and was proposed to regulate mitochondrial orientation within the cell. However, recent evidence suggests a highly dynamic role for CLU in multiple mitochondrial processes. CLU in flies (*Drosophila melanogaster*) negatively regulates the interaction between PTEN-induced putative kinase 1 (PINK1) and Parkin necessary for mitochondrial autophagy [44]. PINK1 and Parkin are mutated in early-onset Parkinson's disease in humans [23]. *CLU HOMOLOG* (*CLUH*) in mice regulates mitochondrial metabolism [42]. Knockout of the *CLUH* homolog in *Arabidopsis*, *FMT* (*FRIENDLY MITOCHONDRIA*), produced alterations in mitochondrial trafficking and matrix exchange [15].

CLU is upregulated in the early stages of development in flies [20] and is upregulated in the liver at birth in mice [42]. *CLUH* is also highly expressed throughout the body in mice with the highest expression in the gut, liver, kidney, heart and testis, and moderate expression in the forebrain and cerebellum [42]. However, the expression of *FMT*, a homolog of *CLU* in plants, remains poorly characterized. *CLUH* is critical to regulate mitochondrial dynamics. Knockout of *CLUH* in *Drosophila* has damaging effects– flies have a decreased lifespan of only 3–7 days, are sterile, and cannot fly [10]. Knockout of *CLUH* in mice is lethal, as $Cluh^{-/-}$ mice die shortly after birth and cannot be rescued [42]. Alternatively, while KO of *Arabidopsis FMT* causes phenotypic abnormalities [15], plants are still functional, mature to flowering, and produce seeds. Since *CLU* is highly conserved between plants and animals, *Arabidopsis* serves as an excellent model to study CLU function. Using this model system, we sought to elucidate the role of this gene, allowing for an understanding of its role in mitochondrial dynamics and behavior with implications for higher organisms.

Results

Expression pattern of *FMT* in *Arabidopsis*

We first investigated organ- and cell-specific expression of *FMT* in *Arabidopsis*. We performed RNA in situ hybridization on various tissue sections using an *FMT*-specific probe. *FMT* transcripts were present at a low level in the vegetative shoot apical meristem (SAM) and surrounding young leaves (Fig. 1A), while *FMT* was highly expressed in the inflorescence and flower meristems (Fig. 1B). *FMT* was also highly abundant in flowers, including carpels and stamens (Fig. 1C–E). In addition, we found that *FMT* transcripts accumulated throughout the mid-stage embryo during the early and late torpedo stages (Fig. 1G, H) but were absent from the mature embryo (Fig. 1I). We included a control probe in the sense orientation, which gave no signal (Fig. 1F). These data indicate a regulatory role for *FMT* in seeds and flower development in *Arabidopsis*.

Generation of overexpression mutants of *FMT* in *Arabidopsis*

To assess the functional role of *FMT* in *Arabidopsis*, we created a transgenic plant line overexpressing (OE) *FMT* (referred to as *FMT-OE*) under the control of the cauliflower mosaic virus (CaMV) 35S promoter. We transformed *Arabidopsis* plants with *Agrobacterium* containing the pFASTG02-FMT overexpression vector. The pFAST vector carries a screenable GFP marker producing a signal detectable in the mature seed coat of transformed plants [45]. We selected transgenic seeds from transformed plants under a fluorescence microscope and identified homozygous T3 lines exhibiting 100% GFP fluorescence compared to wild-type (WT) seeds (Fig. 2A, B). After creating a transgenic line overexpressing *FMT*, we obtained an *fmt* KO line from the Arabidopsis Biological Resource Center (ABRC, Ohio State University, Columbia, OH, USA). Genomic PCR verified this line contained an insertion at the first base of the second intron, preventing correct mRNA splicing [28] (Figure S1). qPCR determined the expression level of *FMT* in both the OE and KO lines. mRNA expression levels were almost two-fold higher in *FMT-OE* plants compared to the

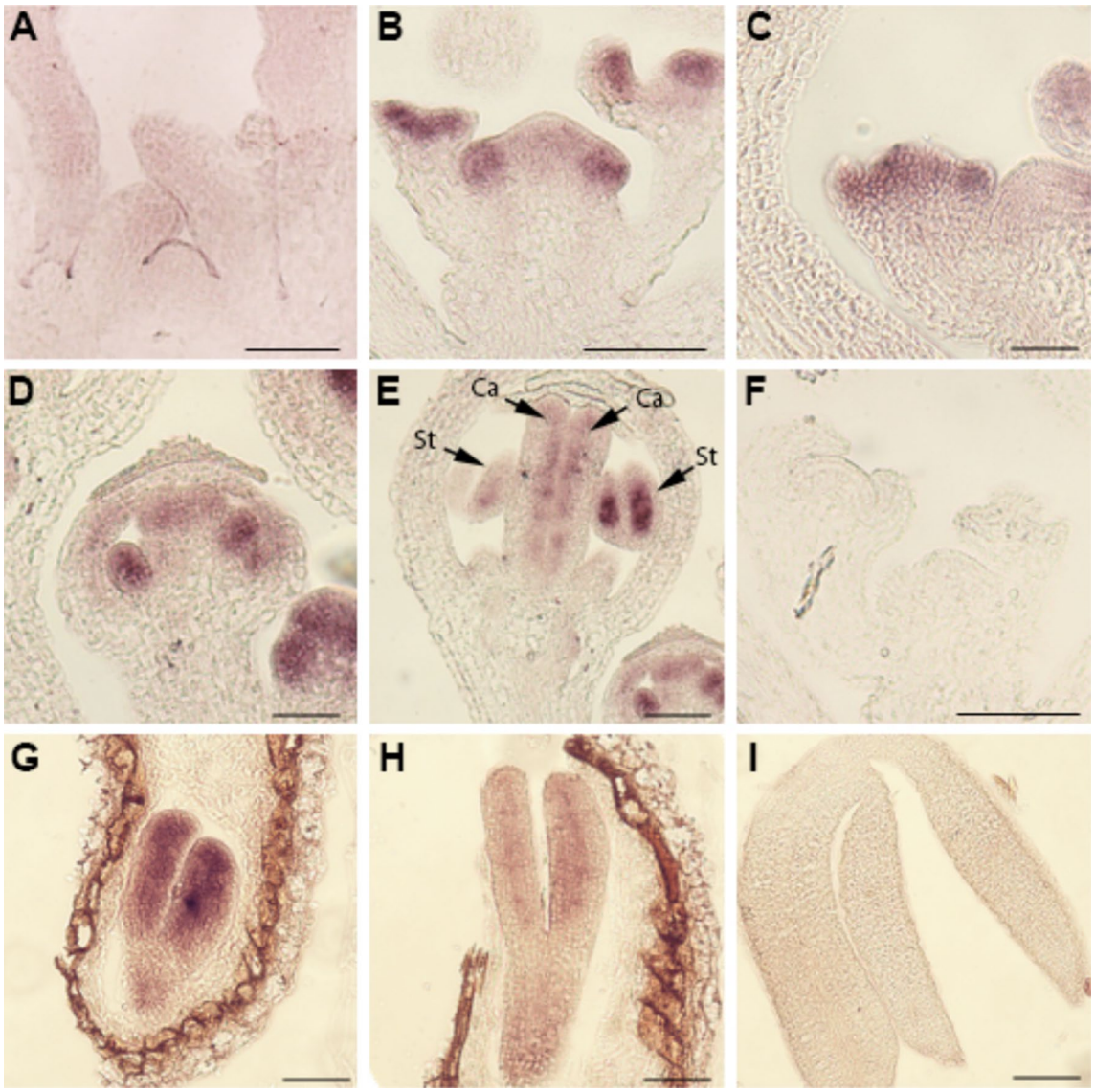

Fig. 1 Expression pattern of *FRIENDLY MITOCHONDRIA (FMT)* in shoot apices, flowers and embryos of *Arabidopsis* Col-0 plants detected by RNA in situ hybridization. Longitudinal sections of vegetative meristem (**A**), inflorescence meristem (**B**), stage 4 flowers (**C**), stage 6 flowers (**D**) and stage 8 flowers (**E**), control probe in sense orientation in longitudinal sections of inflorescence meristem (**F**), embryos at various stages (**G–I**), early torpedo stage (**G**), late torpedo stage (**H**) and mature embryos (**I**). Arrow indicates *FMT* expression in stamen (St) and carpel (Ca) primordia. Scale bar = 100 µm

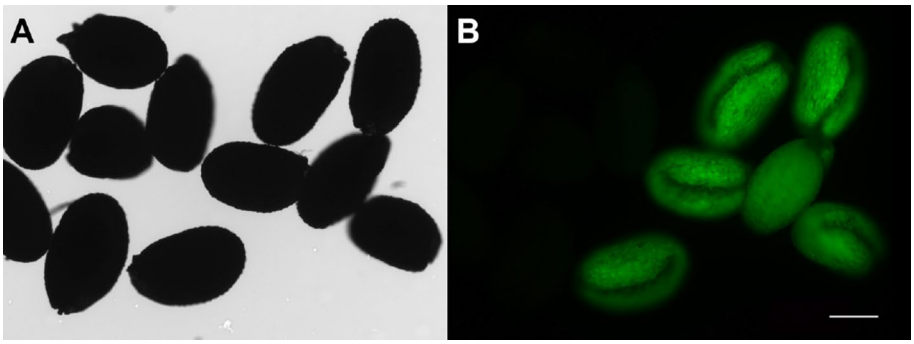

Fig. 2 *Arabidopsis* seeds transformed with pFASTG02-FMT show green fluorescence. **A** Transgenic seeds overexpressing *FMT* in the pFASTG02 vector show green fluorescence (right), while non-transformed WT seeds (left) do not show green fluorescence. **B** Same field of view as in **A**, viewed under bright field light. Scale bar = 100 µm

WT, while there was no detectable expression in the KO line (Figure S2).

FMT affects mitochondrial morphology and dynamics

It was previously shown [15] that *fmt* mutants in *Arabidopsis* exhibit altered morphology, whereby organellar clustering is triggered by a lack of mitochondrial trafficking and motility, both known to be essential for proper cellular function. This phenotype of mitochondrial clustering often occurs under stress conditions, where mitochondria displayed altered motility and distribution [8, 35]. Similar mutants with a non-functional *CLU* showed a significant increase in mitochondrial clustering in a variety of other species, including slime mold, yeast, fruit flies, and mice [10, 17, 18, 42]. Since *fmt* mutants have a significantly smaller root cap than WT plants [15], we analyzed mitochondria in root cap cells 7 days after germination (DAG) by transmission electron microscopy (TEM). We examined mitochondrial morphology and dynamics, including area, aspect ratio (AR), mitochondrial number, membrane fusions and clustering.

We found that plants lacking *FMT* showed a significant increase in mitochondrial number (Fig. 3B, D), although AR and mitochondrial area remained unchanged (Fig. 3E, F). WT and *FMT-OE* plants did not show a statistically significant difference in the number of mitochondria (Fig. 3A, E, D). To analyze mitochondrial dynamics, we examined membrane interaction events of the inner mitochondrial membrane (IMM) and outer mitochondrial membrane (OMM) contacts in WT, *fmt* and *FMT-OE* plants. We found that *fmt* mutants displayed a significant increase in the number

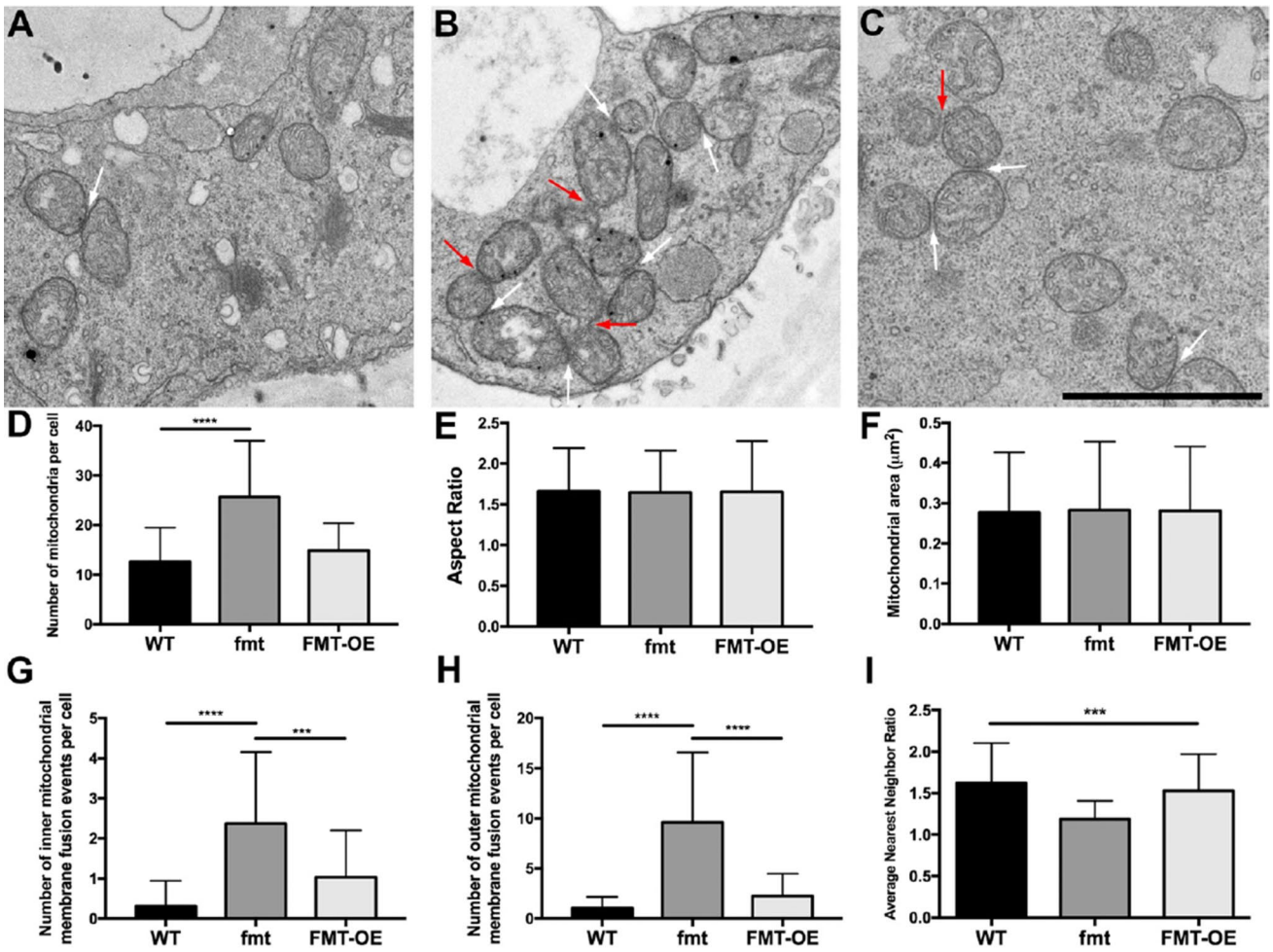

Fig. 3 FMT regulates mitochondrial morphology and dynamics. **A**–**C** TEM of mitochondria from columella cells. Each square represents a 4 μm×4 μm area selected from a representative cell from each genotype: **A** WT, **B** *fmt* and **C** *FMT-OE*. **D** Number of mitochondria per cell from three plant lines. **E** Aspect ratio (AR) from three plant lines. **F** Mitochondrial area (μm^2) from three plant lines. **G** Inner mitochondrial membrane (IMM) fusion events from three plant lines. **H** Outer mitochondrial membrane (OMM) fusion events from three plant lines. **I** Nearest neighbor value (R_n) between three plant lines. Statistical analysis indicates significant differences (****$P \leq 0.0001$, ***$P \leq 0.001$, *$P \leq 0.05$) using one-way ANOVA. Bars and error bars represent mean and standard deviation, respectively. Scale bar = 2 μm

of IMM fusion events compared to both WT and *FMT-OE* (Fig. 3G). In addition, *fmt* mutants also displayed a significant increase in the number of OMM fusion events compared to both WT and *FMT-OE* (Fig. 3H). We then used the nearest neighbor value (R_n) to examine mitochondrial clustering in root cap cells. We found that mitochondria in plants lacking *FMT* trended towards clustering, while the mitochondria of WT and *FMT-OE* plants trended towards dispersion (Fig. 3I). Taken together, our data confirmed previous findings [15] and provides additional evidence that *FMT* regulates various mitochondrial mechanisms, including mitochondrial number, clustering, and inner and outer mitochondrial membrane fusions.

FMT affects seedling germination and germination timing

We next examined whether these changes in mitochondrial dynamics led to developmental, phenotypic, or behavioral changes in the whole plant. Seeds undergo numerous metabolic changes during development and maturation, including distinct changes in tricarboxylic acid (TCA) cycle and β-oxidation metabolites [16]. Mitochondria undergo dynamic changes during seed germination, including a reactivation of metabolism and increased mitochondrial motility [37]. Because our data showed that *FMT* is highly expressed during the mid-stages of embryogenesis (Fig. 1C–E, G, H), we analyzed the effects of both *FMT-OE* and *fmt* KO on germination. We measured germination timing and germination rate on Murashige–Skoog (MS) agar plates. We found that *FMT-OE* seedlings took between 72 and 96 h to germinate, while WT and *fmt* seedlings germinated within 24–48 h (Fig. 4A, B). In addition, the germination rate of the *FMT-OE* line was significantly decreased (~85%) compared to WT and *fmt* seeds (~98%), which indicates that *FMT* also negatively regulates germination rate (Fig. 4C). These data reveal a previously unknown role of FMT in regulating germination in *Arabidopsis*.

FMT affects root length and flowering timing in *Arabidopsis*

fmt mutants in *Arabidopsis* were previously described as having significantly shorter roots than the WT, likely resulting from their smaller meristematic zones [15]. This suggests that *FMT* functions as a regulator of root length, particularly within the meristematic zone. Therefore, we examined if *FMT* overexpression increased root length when grown on MS agar plates. At 7 days after germination (DAG), we found that both *fmt* and *FMT-OE* plants had significantly shorter roots than the WT (Fig. 5A, B). Although the roots of *fmt* mutants were still significantly shorter than the WT at 14 DAG, the roots of *FMT-OE* mutants overcame an initial deficit in root length and were comparable to those of the WT (Fig. 5C, D). These results confirm previous findings [15] and further demonstrate a clear role for *FMT* in regulating and maintaining root growth and length.

Since we demonstrated that *FMT* is expressed in the inflorescence shoot apical meristem and the flower structure (Fig. 1), we examined the effect of *FMT* on flowering timing in *Arabidopsis* under long-day (16 h light/8 h dark) conditions. We defined flowering time of WT, *fmt* and *FMT-OE* as the time point of the emergence of the first visible floral stem (bolting) and the number of rosettes leaves at the time of flowering. We found that *fmt* plants exhibited a significant delay in flowering timing, taking on average between 33 and 34 days to flower, compared to 28–29 days in the WT and 29–30 days in *FMT-OE* plants (Fig. 5E, F). In addition, we found that *fmt* mutants had a significant increase in the number of leaves at the time of flowering compared to WT and *FMT-OE* plants (Fig. 5G). Generally, the rosette leaf number reflects the timing of flowering. We found an increase in leaf number in *fmt* mutants that positively correlated with

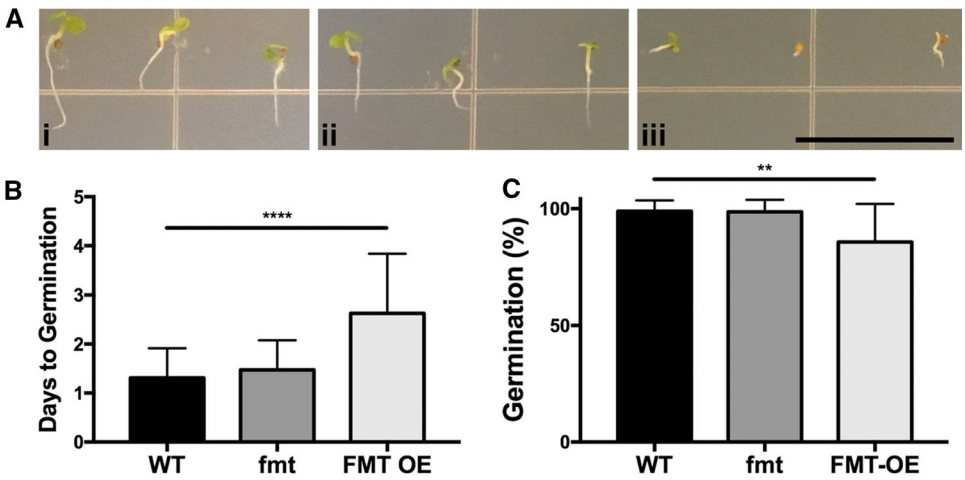

Fig. 4 FMT regulates germination timing and total germination. **A** Plants 4 days after germination (DAG), (i) WT, (ii) *fmt* and (iii) *FMT-OE*. **B** Quantification of days to germination. **C** Quantification of germination rate (in %). Scale bar = 1 cm. Statistical analysis indicates significant differences (****$P \leq 0.0001$, **$P \leq 0.01$) using one-way ANOVA. Bars and error bars represent mean and standard deviation, respectively

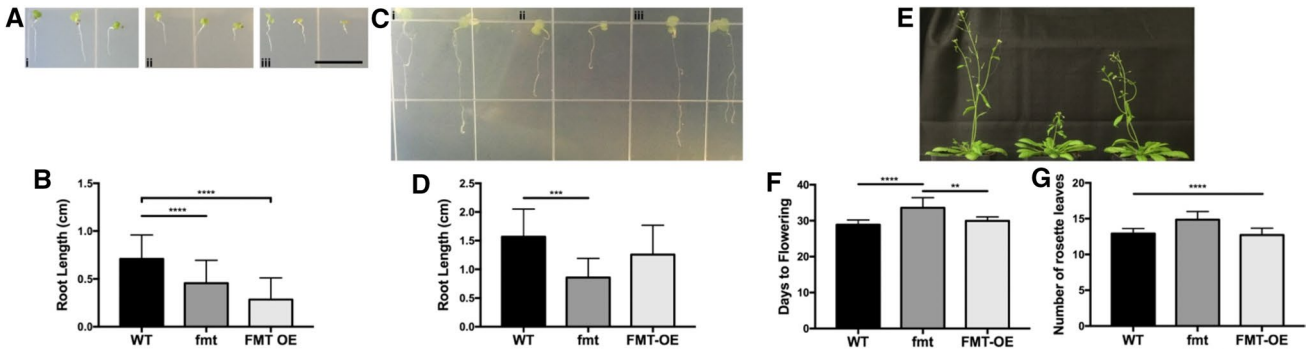

Fig. 5 FMT regulates root length and flowering timing under long-day conditions. **A** Root length at 7 DAG, (i) WT, (ii) *fmt* and (iii) *FMT-OE*. **B** Quantification of root length at 7 DAG. **C** Root length at 14 DAG in (i) WT, (ii) *fmt* and (iii) *FMT-OE*. **D** Quantification of root length at 14 DAG. E) Flowering time phenotype at 35 DAG, (i) WT, (ii) *fmt*, (iii) *FMT-OE*. **F** Quantification of days to flowering. Scale bar = 1 cm. Statistical analysis indicates significant differences (****$P \leq 0.0001$, ***$P \leq 0.001$, **$P \leq 0.01$) using one-way ANOVA. Bars and error bars represent mean and standard deviation, respectively

the late flowering time phenotype of the mutant. Our data indicate that *FMT* is necessary for normal flowering in the *Arabidopsis* WT, where it acts as a positive regulator of flowering timing.

FMT affects the salt stress response in *Arabidopsis*

Plants exhibit several behavioral responses to salt stress, including inhibition of germination, delay in flowering timing, disrupted root growth, and salt avoidance tropism [14, 26, 40, 47, 48]. Since *FMT* regulates mitochondrial morphology and dynamics, we tested whether salt stress-responsive behaviors were altered in our mutants. Using the spatio-temporal root stress browser [13], we were able to examine expression levels in roots of five-day-old *Arabidopsis* Col-0 seedlings exposed to 140 mM NaCl for 48 h. *FMT* showed an increased expression in the epidermal cell layer 3 h after exposure to NaCl, with peak expression after 32 h. This expression remained elevated up to 48 h after exposure to NaCl compared to non-stressed control plants (Fig. 6A). These data reveal a previously unknown role for *FMT* as a salt-responsive gene in *Arabidopsis* and indicate a major regulatory role for *FMT* in *Arabidopsis* in this physiological response. Following salt stress, plants typically decrease primary root growth to minimize root exposure to excess Na^+ [34]. To determine the effects of salt stress on our mutants, plants from all three lines were germinated and grown on MS agar plates for seven days, and then transferred to MS agar plates supplemented with 125 mM NaCl for seven days. We recorded root length on the seventh day. We found that both WT and *FMT-OE* plants exhibited a significant decrease in primary root length upon exposure to salt stress (Fig. 6F, H), while primary root length in *fmt* mutants remained unchanged (Fig. 6G). Taken together, these data provide evidence that *FMT* regulates salt stress-induced phenotypes, including germination, flowering timing, and primary root growth.

Excess salt in the soil is first sensed by the root cap, which transmits signals to the rest of the plant to induce salt-responsive behaviors [12]. We examined whether altered mitochondrial dynamics in the root cap could explain these differences in behavior, since *FMT* is expressed in the root and up-regulated during salt stress, and the mutants exhibited an altered response to salt stress. Using TEM, we analyzed mitochondria in root cap cells of our three lines after exposure to 125 mM NaCl stress. We found that the number of mitochondria per cell increased significantly in WT and *FMT-OE* plants upon salt stress, but remained unchanged in *fmt* (Fig. 7D–F). The number of IMM contacts decreased significantly in *FMT-OE* plants during salinity stress, but was not affected in WT or *fmt* (Fig. 7G–I). In addition, OMM fusion events were not affected by salt stress in any of the three lines (Fig. 7J–L). After salt stress, mitochondria trended towards dispersion in the WT, clustering in *FMT-OE* plants, while *fmt* remained unchanged compared to WT (Fig. 7M–O). Total mitochondrial area remained unchanged in *fmt* mutants following salt exposure (Figure S4, A–C), while mitochondrial aspect ratio decreased significantly in all three lines (Figure S4, D–F). These results indicate that *FMT* regulates various aspects of mitochondrial dynamics and morphology under salt stress conditions. Altering this regulation could induce changes in the salt stress response of the mutants.

We further tested germination rate and timing of WT, *fmt* and *FMT-OE* plants under salt stress conditions. We sowed seeds on MS agar plates supplemented with 125 mM NaCl. We found that germination rate was significantly decreased by ~ 50% in *FMT-OE* seeds compared to WT and *fmt* (Fig. 6B). Seeds of *FMT-OE* plants took significantly longer to germinate (~ 6 days) than seeds from WT and *fmt* plants

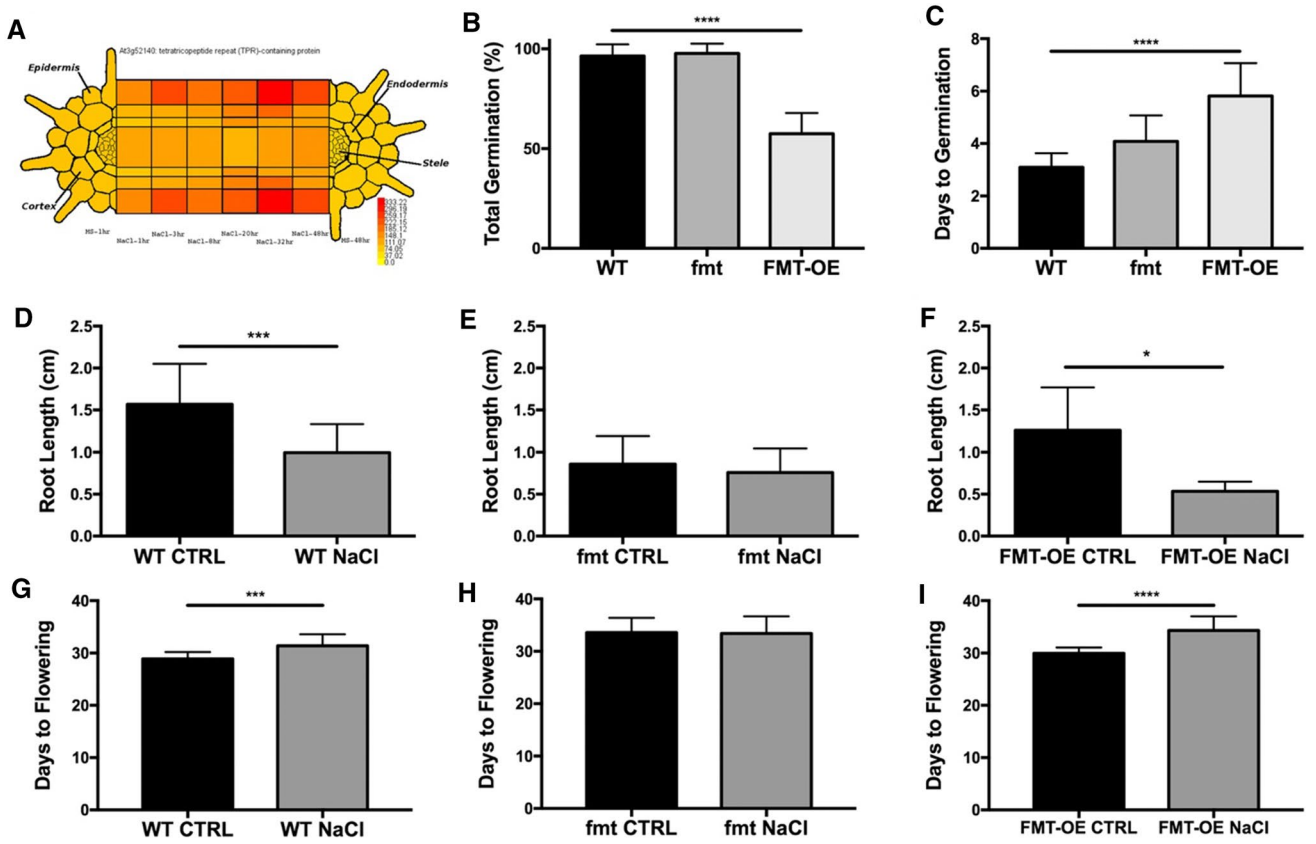

Fig. 6 FMT affects the response to salt stress in *Arabidopsis*. **A** Spatio-temporal root stress browser of *FMT* expression in response to 140 mM NaCl over 48 h. Control (MS) expression at 1 and 48 h provided on the left and right root cross-sections, respectively. Gene expression level is directly compared to the highest signal record for the given gene (*FMT*) and assigned an accompanying color, ranging from yellow (no expression) to red (highest/absolute) expression. **B** Quantification of total germination (in %). **C** Days to germination. **D** Primary root length under control and salt-stress conditions in WT. **E** Primary root length under control and salt-stress conditions in *fmt*. **F** Primary root length under control and salt-stress conditions in *FMT-OE*. **G** Days to flowering under control and salt-stress conditions in WT. **H** Days to flowering under control and salt-stress conditions in *fmt*. **I** Days to flowering under control and salt-stress conditions in *FMT-OE*. Black bars indicate control conditions. Gray bars indicate exposure to 125 mM NaCl. Statistical analysis indicates significant differences (****$P \leq 0.0001$, ***$P \leq 0.001$, *$P \leq 0.05$) using one-way ANOVA. Bars and error bars represent mean and standard deviation, respectively

(Fig. 6C). Of note, salt treatment affects germination rate and flowering timing of *FMT-OE* plants to a greater degree than observed under normal (non-stress) conditions (see Fig. 4). The *FMT-OE* plants germinated in ~ 4 days under non-stress conditions (Fig. 4A), while showing delayed germination by approximately two days under salt treatment (Fig. 6C). We observed a similar response for germination rate, which was affected by 50% under stress in *FMT-OE* plants (Fig. 6B) compared to ~ 89% under normal conditions (Fig. 4C). The *fmt* mutant displayed an insensitivity to salt treatment, showing a WT-like germination rate. However, the days to germination was also significantly increased in *fmt* compared to WT plants. Total germination rate remained unchanged compared to control conditions (Figure S3). Our above results demonstrated that *FMT* acts as a negative regulator of germination under normal conditions in *Arabidopsis*. In the presence of salt treatment, we found an enhanced stress response in *FMT* overexpression plants, which further delayed seed germination compared to control conditions. These results demonstrate that salt stress influences the germination process through the *FMT* gene.

We next exposed 1-week-old seedlings to 125 mM salt stress on soil and recorded the days to flowering for each of the three lines. We found that both WT (Fig. 6G) and *FMT-OE* plants (Fig. 6I) took significantly longer to flower under salt stress, defined as the days to emergence of the first visible floral stem, than *fmt* mutants. Notably, salt stress did not delay flowering of *fmt* mutants compared to control conditions (Fig. 6H).

Salt stress can affect flowering timing depending on the salt concentration [40, 41]. So, we sought to define when the floral transition took place in WT plants grown under salt stress. We performed toluidine blue staining on longitudinal sections of apices of Col-0 plants grown under

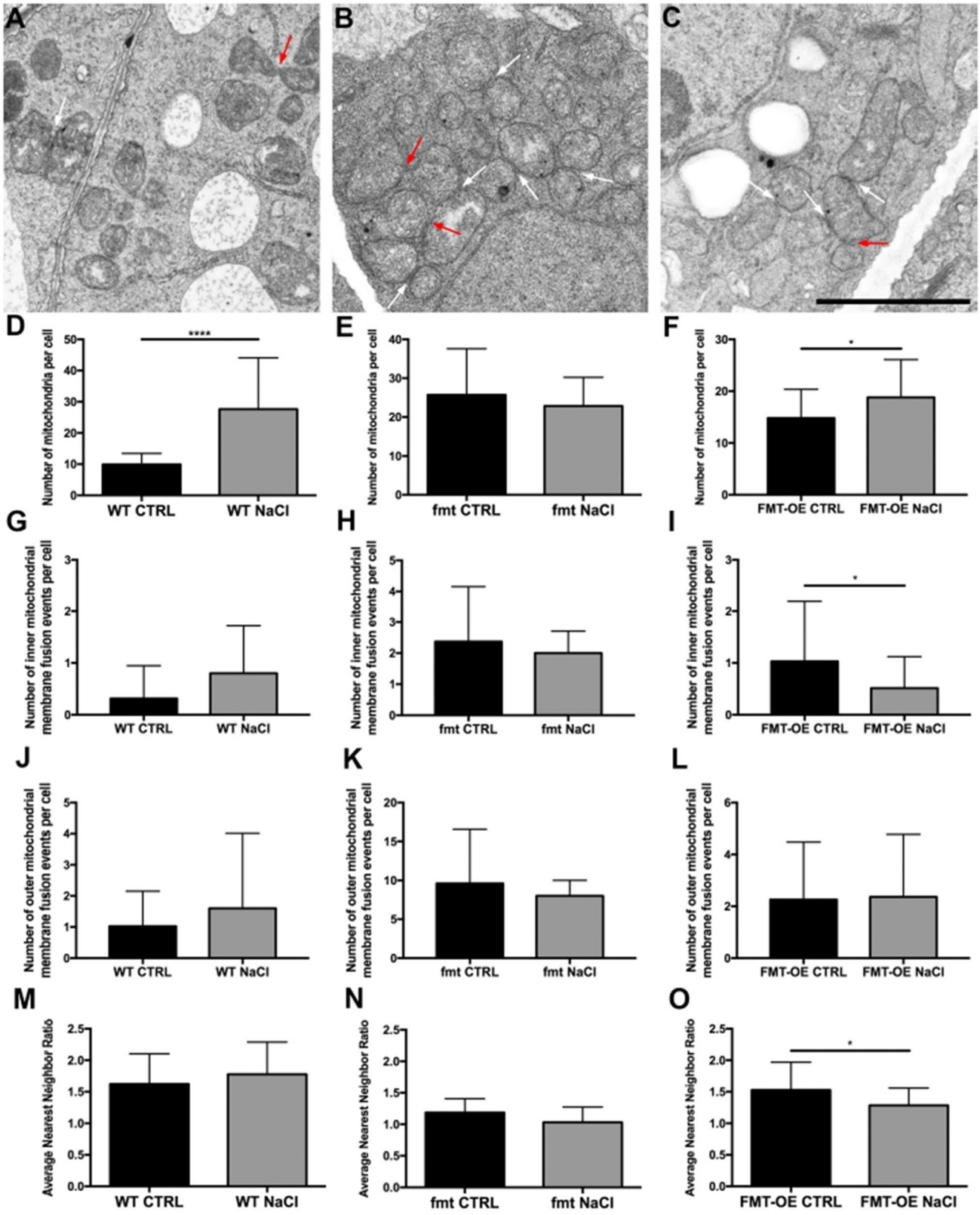

long days and harvested at 0, 1, 2 and 3 days after transfer (DAT) to salt media (Fig. 8A–H). As expected, WT plants grown under control conditions initiated the floral transition faster (1 DAT) (Fig. 8B) than the salt grown plants (3 DAT) (Fig. 8H). To delineate the role of *FMT* during salt exposure, we analyzed the expression of *FMT* in the SAM of

◂**Fig. 7** FMT regulates mitochondrial morphology and dynamics under salt stress. **A–C** TEM of mitochondria from columella cells. Each square represents a 4 µm × 4 µm area selected from a representative cell from each genotype: **A** WT, **B** *fmt* and **C** *FMT-OE*. **D–F** Number of mitochondria per cell in plants under salt stress compared to control conditions in WT, *fmt*, and *FMT-OE*, respectively. **G–I** Number of inner mitochondrial membrane fusion events in plants under salt stress compared to control conditions in WT, *fmt*, and *FMT-OE*, respectively. **J–L** Number of outer mitochondrial membrane fusion events in plants under salt stress compared to control conditions in WT, *fmt*, and *FMT-OE*, respectively. **M–O** Average nearest neighbor ratio in in plants under salt stress compared to control conditions in WT, *fmt*, and *FMT-OE*, respectively. Statistical analysis indicates significant differences (****$P \leq 0.0001$, *$P \leq 0.05$) using one-way ANOVA. Bars and error bars represent mean and standard deviation, respectively

WT plants grown in control and salt conditions (125 mM NaCl) by RNA in situ hybridization using *FMT* as a probe. We analyzed longitudinal sections of apical meristems of plants grown under either normal or salt stress conditions, harvested at end of day (ED) at 0, 1 and 2 DAT to salt media (Fig. 8I–N). We detected transcripts of *FMT* at a low level in the vegetative SAM of WT plants grown in both conditions at 7 DAG (0 DAT) (Fig. 8I, L). Interestingly, *FMT* expression was highly induced during floral transition in the SAM and young leaves at 1 DAT in WT plants grown in control conditions (Fig. 8J). *FMT* transcript abundance initially declined after shifting plants to salt media (Fig. 8M) and then recovered, as we detected the *FMT* transcript level in the SAM of salt treated plants at 2 DAT (Fig. 8N). These data provide evidence that salt exposure decreases *FMT* expression in the SAM. Our observed delay in flowering time of WT and *FMT-OE* plants grown in salt media may reflect decreased *FMT* expression upon exposure to salt. Thus, our data indicates that *FMT* is an essential regulator of flowering timing and a potential target of salt-affected flowering. Taken together, these data provide evidence that *FMT* regulates salt stress-induced phenotypes, including germination, flowering timing, and primary root growth.

FMT affects plant size by regulating leaf expansion growth

Since *fmt* mutants show a reduced plant size [15], we tested whether *FMT* regulates leaf expansion growth using an established phenotyping system (Phytotyping^{4D}) [1]. We imaged eight WT, ten *fmt*, and eight *FMT-OE* plants using the Phytotyping^{4D} system for eight consecutive days (from 15 to 23 days after sowing, DAS) at a time resolution of five images per hour per plant (Fig. 9A, Supplemental Movie S1). During this time, all three genotypes showed an exponential increase in rosette area, but *fmt* plants were approximately 25% smaller ($P < 0.05$, Student's *t* test), and *FMT-OE* were approximately 35% smaller ($P < 0.01$, Student's *t* test) compared to the WT at 23 DAS. The time series from the eight 24-h-cycles were combined to calculate the diurnal changes in the relative expansion rate (RER) (Fig. 9B, C). Generally, the diurnal RER of the three lines resembled those reported previously [1]. RER decreased after dawn, peaked around 4 h, and then stayed fairly constant for the remainder of the day with a peak directly after dusk. We found only marginal diurnal differences among the three lines. For example, there were slight variations in RER timing, as *fmt* mutants had a significantly enhanced RER peak at 4 h after dawn compared to WT and *FMT-OE*.

FMT affects hyponastic behaviors

Behavior has been defined as: "what a plant or animal does, in the course of an individual's lifetime, in response to some event or change in its environment" [46]. This definition is not intended to assume that all behaviors exhibited by animals are also present in plants and vice versa; rather, it comprises a more comprehensive definition to encompass the range of overlap between the behaviors of plants and animals in response to their environments. We can classify these behaviors based on various activities, such as growth (of an individual plant or animal), irreversible change (seed germination in plants or imprinting in animals), flexible change [movements based on circadian clocks in both plants (nyctinasty/hyponasty) and animals (sleep/wake cycle)], or response to stress (avoidance in both plants and animals).

We evaluated the behaviors of our three plant lines by examining movements, i.e. mobility based on the circadian clock, and stress-responsive behaviors, which can be accurately detected and measured. Hyponastic movement of *Arabidopsis* leaves follows a pattern of rhythmic, diurnal oscillation driven by the circadian clock [31], which is measured as the change in leaf angle over time [33]. We employed the Phytotyping^{4D} system to determine the hyponastic behavior of leaves by tracking their average hyponastic angles from 15 to 23 DAS. We found that WT plants exhibited a high leaf angle during the night, which decreased after dawn, and then increased at dusk and throughout the night. These results are consistent with previous reports from Apelt et al. [1] and [2]. In our tested transgenic and mutant lines, we saw a consistently higher hyponastic angle in *FMT-OE* plants, while *fmt* mutants displayed a consistently lower hyponastic angle (Fig. 10A). This finding was even more pronounced when incorporating the diurnal average of the hyponastic angle over the whole time series (Fig. 10B, C). *fmt* mutants showed a temporal delay of leaf angle increase after dusk and lower angles during the night. We also found significant differences in the speed of leaf movement between the fmt mutant and WT and *FMT-OE* plants after dusk and during the first half of the day

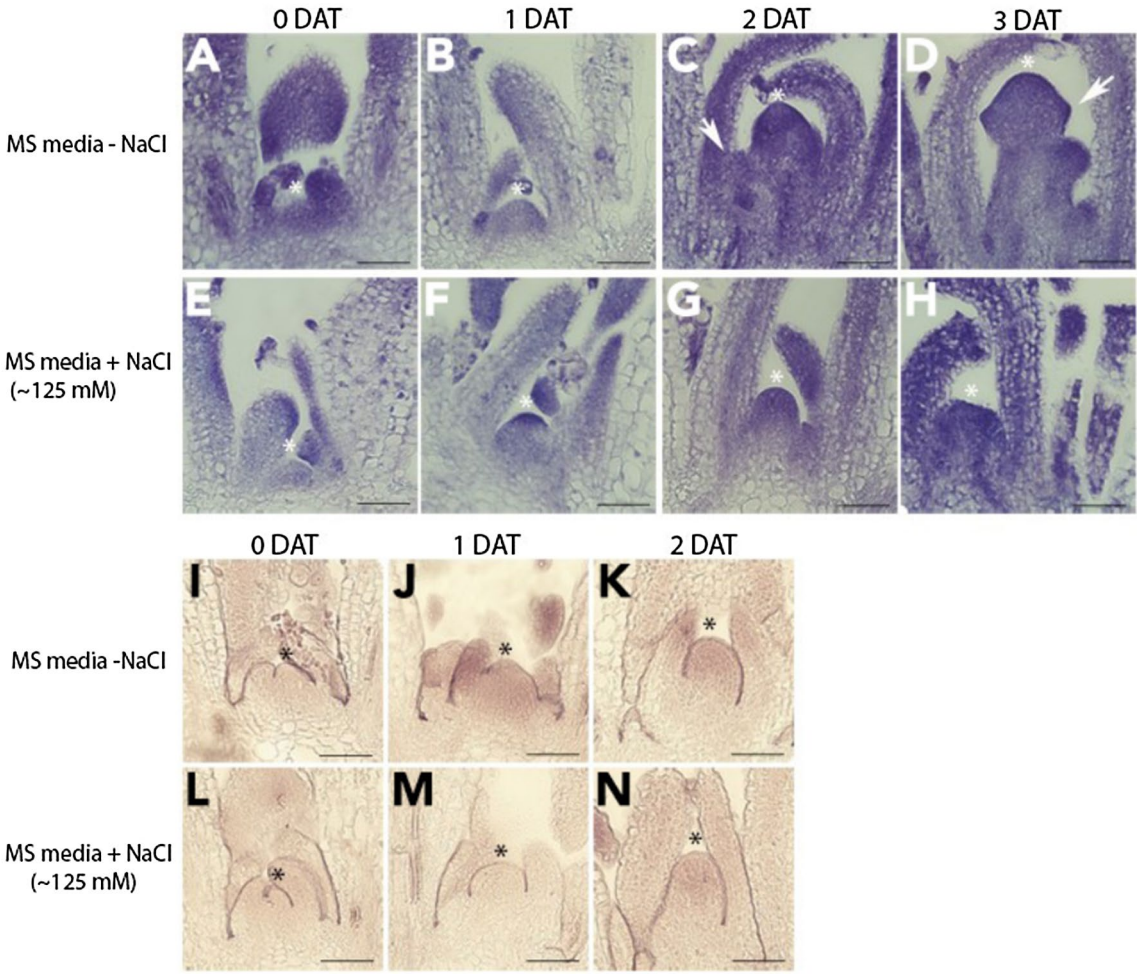

Fig. 8 Salt treatment delays floral transition in Col-0 plants and affects *FMT* expression in the shoot apical meristem. **A**–**H** Emergence of flower primordia analyzed by toluidine blue staining from apices of Col-0 plants grown under long days and harvested at 0, 1, 2 and 3 days after transfer (DAT) to salt media. **I**–**N** RNA in situ hybridization using *FMT* as a probe on longitudinal sections of the apical meristem of shifted plants grown in normal and salt conditions, harvested at end of day (ED) at 0, 1 and 2 days after transfer (DAT). Asterisks and arrows indicate meristem summit and floral primordia, respectively. Scale bars = 100 µm

(Fig. 10D, E). These data demonstrate an important role for *FMT* in regulating hyponastic behavior, including changes in speed of leaf movements.

Knockout of CLUH in mice affects mobility and speed

The homolog of FMT in mice, clustered mitochondria homolog (CLUH), has previously been shown to bind nuclear-encoded mitochondrial mRNAs [18]. However, the effects of CLUH on behavior in mice has yet to be reported. To examine whether CLUH may have behavioral effect in mice corresponding to the effect of *fmt* in *Arabidopsis*, we studied whole body heterozygous (HET) *Cluh*$^{\pm}$ mice [42]. There were no observable differences in bodyweight between WT and *Cluh*$^{\pm}$ mice of either sex at 8 weeks of age (Figure S5). We performed several behavioral tests, including marble burying, open field, and zero maze on 18 WT and 17 HET mice. We found no significant differences in the marble burying test or zero maze test (data not shown). However, we observed significant differences between WT and heterozygous mice in the open field test. We found that heterozygous mice travelled for shorter distances (Fig. 11A), and had a slower average and maximum speed (Fig. 11B, C, respectively). These results unmask a conserved and overlapping influence of *fmt* and CLUH on speed of movement of plants and animals, respectively (Fig. 11D).

Discussion

Mitochondria are highly conserved organelles essential for the health of both plants and animals. They regulate numerous critical processes, such as energy production, cellular

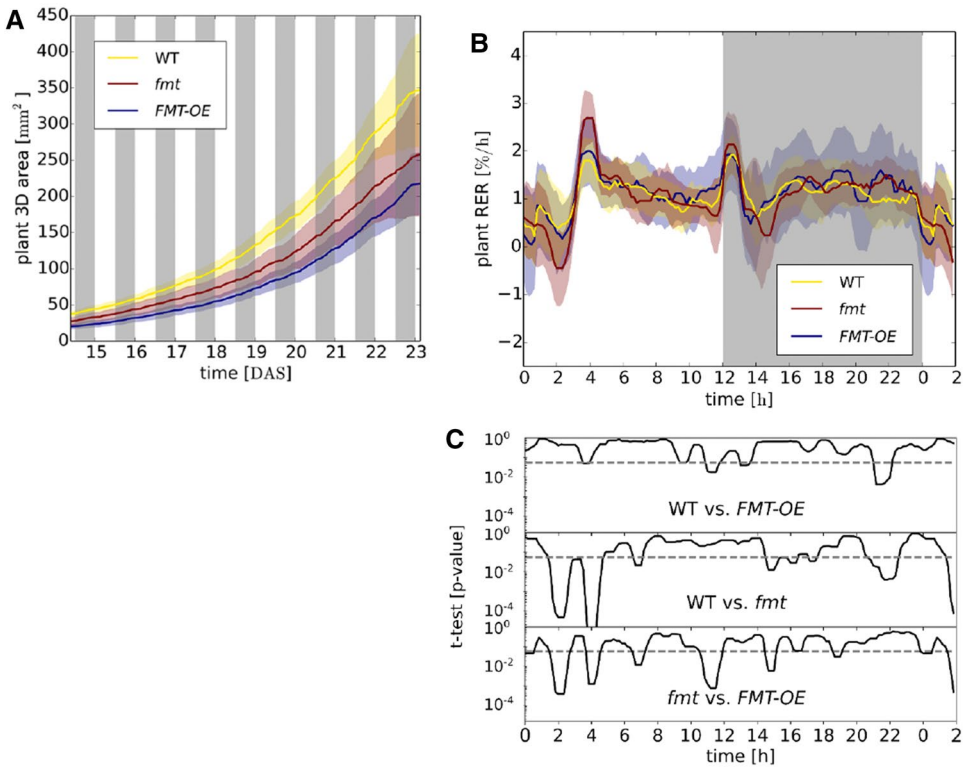

Fig. 9 *fmt* and *FMT-OE* mutants exhibit changes in spatio-temporal growth. **A** Rosette area increased over time (15–23 days after sowing, DAS) determined by 3D imaging. Yellow: WT, red: *fmt*, blue: *FMT-OE*. **B** Diurnal relative expansion rate (RER) averaged over eight sequential 24-h periods. **C** *p* values from pairwise Student's *t* tests applied over a 50-min sliding window, where *p* values < 0.05 indicated significance. Lines and color-shaded areas represent mean and standard deviation, respectively. Plants grown in a 12 h photoperiod

metabolism, and apoptosis, among others [7, 9, 30]. Mitochondrial dysfunction is implicated in underlying multiple physiological and pathological behaviors in higher organisms and hallmark behaviors of multiple neurodegenerative diseases, including Alzheimer's disease, Parkinson's disease, schizophrenia, Williams syndrome and autism spectrum disorders [4, 5, 21, 22, 24, 25, 36, 38]. Plants and animals share numerous homologous genes encoding mitochondrial proteins that are in themselves highly functionally conserved, including *CLU*, a gene originally thought to mediate mitochondrial localization [17, 56]. However, we now know that CLU plays multiple important roles within the cell, including regulating mitochondrial autophagy through the interaction between PINK1 and Parkin [44], mitochondrial metabolism [42] and directing mitochondrial trafficking [15]. *FMT*, the functional homolog of *CLU* in *Arabidopsis*, regulates not only various aspects of mitochondrial morphology and dynamics within the cell, as well as plant development [15], but also hyponastic and salt stress-responsive behaviors.

We confirmed previous findings that *fmt* mutants exhibit altered mitochondrial morphology and dynamics, hence *FMT*-deficient plants show a significantly increased number of mitochondria and display more clustered mitochondria [15]. Mitochondria of *fmt* mutants also show more connections with each other, either through inner or outer mitochondrial membrane contacts. However, we found also that under salt stress conditions, the number of mitochondria per cell increased significantly in WT and *FMT-OE* plants but remained unchanged in *fmt* mutants. These results reveal a vital role of *FMT* in regulating mitochondrial morphology and dynamics under both control and salt stress conditions.

We also observed that a heterozygous knockout of CLUH affects mouse mobility and speed. Interestingly, a knockout of FMT also affected speed and leaf movement in *Arabidopsis*. This suggests there may be a conserved role for this gene in regulating speed of movement in plants and animals. Behaviors such as speed are one of many fundamental ways an organism responds to its environment. These behaviors are driven by changes in cellular and molecular mechanisms that then drive changes in various physiological processes through which phenotypic and developmental changes emerge. An alteration of these cellular and molecular mechanisms often results in fundamental changes that can lead to changes in behavior or, ultimately, disease. Any insight into how these fundamental cellular processes work can lead to a better understanding of these behaviors and disease mechanisms. Although plant species such as *Arabidopsis* are not routinely used to study human diseases or behaviors, they contain several highly conserved genes and fundamental processes that are similar to animals. This suggests that *Arabidopsis* can serve as a complementary model organism for disease or behavioral research.

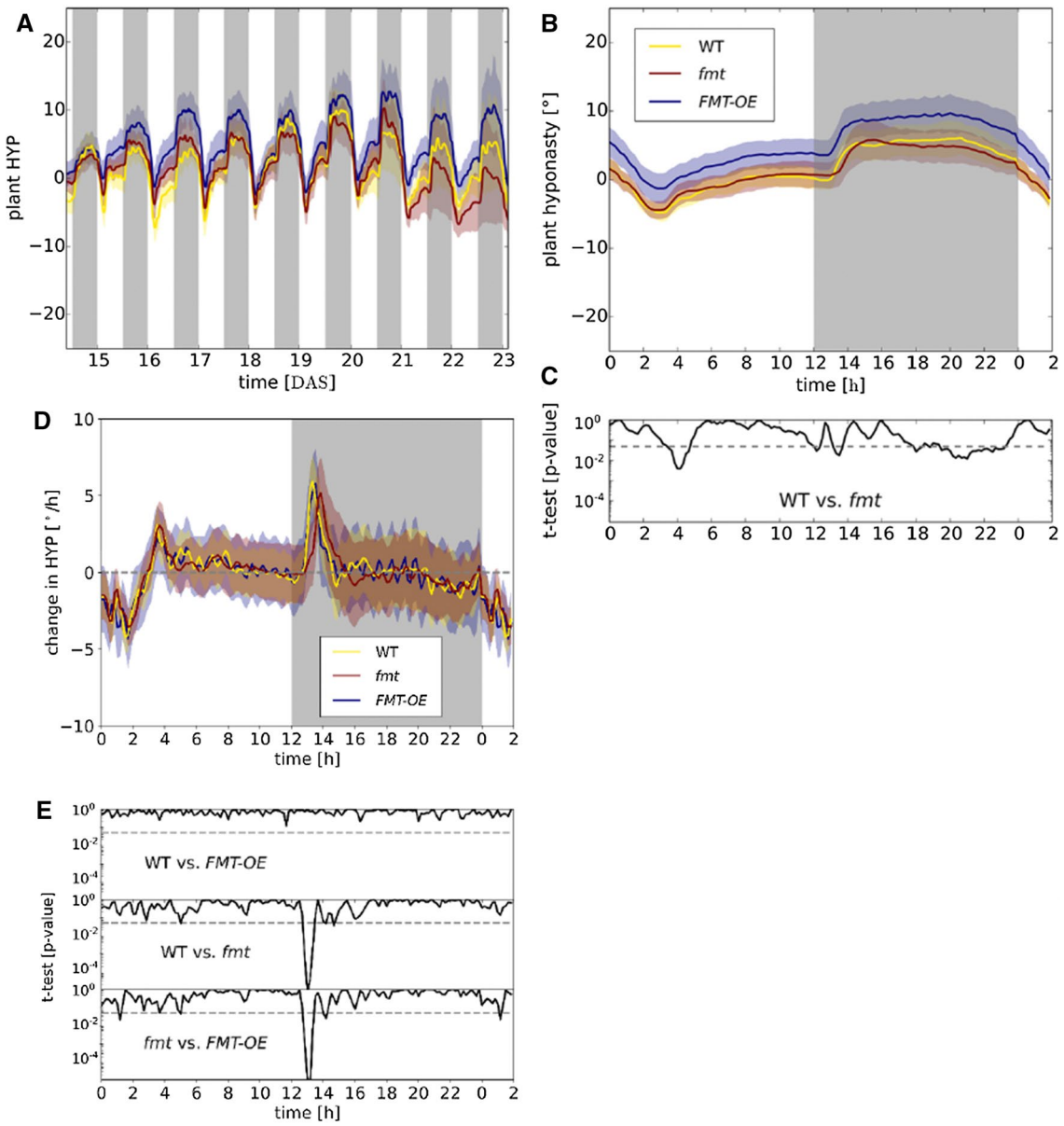

Fig. 10 FMT regulates hyponastic growth in *Arabidopsis*. **A** Average hyponastic angle (HYP) over time (15–23 DAS). **B** Diurnal HYP averaged over eight sequential 24-h periods. **C**, **E** *p* values from pairwise Student's *t* tests applied over a 50 min sliding window, where *p* values < 0.05 indicated significance. **D** Change in speed of hyponastic angle (HYP) averaged over eight sequential 24-h periods. Lines and color-shaded areas represent mean and standard deviation, respectively. Plants grown in a 12 h photoperiod

Materials and methods

Plant materials and growth conditions

All experiments were done using Arabidopsis (*Arabidopsis thaliana*) in the Columbia-0 (Col-0) ecotype. Seeds were surface sterilized by washing in 70% (v/v) ethanol for 5 s, and this wash was replaced by 0.1% triton X-100 in 50% household bleach (v/v) for 5 s before five rinses in sterile distilled water. Seeds were then plated on 100 × 100 × 15 mm square petri dishes (Ted Pella) filled with MS-agar, and plates were stratified at 4 °C for three days in the dark to synchronize germination. Plates were then moved to long-day photoperiod conditions at 22 °C ± 1 °C under cool-white light at 100 µmol m^{-2} s^{-1}. Plates were placed at an angle to allow for root growth along the surface of the agar. For salt-stressed growth conditions on plates, seeds were plated on MS-agar plates supplemented with 125 mM NaCl. For experiments done in soil, Arabidopsis seeds were stratified before direct sowing on Fafard #2 soil mixture (Sun Gro Horticulture).

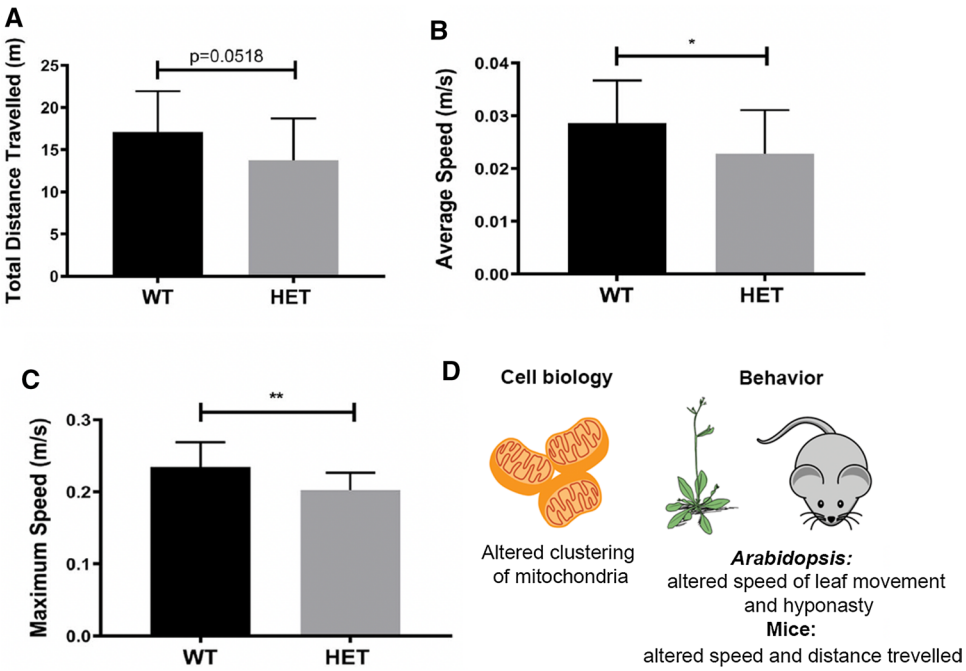

Fig. 11 CLUH affects mouse mobility and speed. **A** Comparison of WT and heterozygous (HET) *Cluh*$^{\pm}$ mice in open field tests: **A** total distance travelled, **B** average speed, **C** maximum speed. **D** Schematic illustration of the homology between *Arabidopsis* and mice regarding the effect of altered clustering of mitochondria

T-DNA insertions lines

FMT was screened for available T-DNA insertion lines on TAIR (The Arabidopsis Information Resource, http://www.arabidopsis.org/). PCR was used to test whether the T-DNA was inserted at the predicted insertion site. All T-DNA insertions were confirmed via PCR using left and right primers flanking the genomic sequence, and a border primer located within the T-DNA sequence (Table 1).

FMT cloning

pFASTG02-FMT was constructed by subcloning a *FMT* cDNA fragment of the expected size into the pDONR 221 vector (Gateway, Invitrogen). To PCR amplify the cDNA fragment, the following primers were used: forward (attB1FPFMT), 5′-GGGGACAAGTTTGTACAAAAAAGCAGGCTTCATGGCTGGGAAGTCGAAC-3′, and reverse (attB1RPFMT), 5′-GGGACCACTTTGTACAAGAAAGCTGGGTCTTTTTTGGCTTTTTGCTTCTT-3′. The fragment was subsequently cloned into pFASTG02 [45] according to the manufacturer's protocol (Invitrogen). This vector construct, pFASTG02-FMT, allowed for overexpression of the *FMT* gene under the control of the cauliflower mosaic virus (CaMV) 35S promoter. The construct was sequenced to identify an error-free clone and subsequently transformed into wild type Col-0 plants by means of *Agrobacterium*-mediated transformation using the *Agrobacterium tumefaciens* strain GV3101 using the floral dip method with the following modifications: Silwet L-77 was added to the sucrose solution to a volume of 0.05% (v/v). The pFAST vector carries a screenable GFP marker producing a signal detectable in the mature seed coat of transformed plants. Lines with a single transgene insertion were identified by an ~ 3:1 segregation ratio of GFP to no-GFP, respectively, using a Zeiss Axioplan 2 fluorescence microscope (Carl-Zeiss, Germany). Transgenic GFP seeds from these lines were sown to identify a homozygous plant (FMT-3), which was identified by T_3 seed that exhibited 100% GFP fluorescence compared to WT seed. Seeds from line FMT-3 were collected and used in subsequent experiments.

For germination experiments, Arabidopsis seeds were plated on square petri dishes containing MS-agar with or without supplementation of 125 mM NaCl. Total germination was recorded 7 days after sowing. For quantification of root length under control conditions, Arabidopsis plants were grown on control MS-agar plates and roots were measured using a ruler at days seven and fourteen. For quantification of root length under salt-stressed conditions, Arabidopsis plants were grown

Table 1 T-DNA primers used in this study

Primer Name	Sequence (5′ → 3′)	Notes
LBb1.3	ATTTTGCCGATTTCGGAAC	Left border primer for T-DNA insertion
FMT LP	ATACCTGCAGCAGTTTGCAAC	Left primer for *FMT* (SALK_046271C)
FMT RP	CTAGCGCCAACAGCTCTACTG	Right primer for *FMT* (SALK_046271C)

on control MS-agar plates for one week, and then transplanted to either control or 125 mM NaCl MS-agar plates for one week and roots were measured at day fourteen. For MS-agar plate experiments, at least 20 replicates were used for each experiment, and each experiment was repeated three times.

Flowering time analysis

For flowering timing experiments, plants were grown on soil in LD at 22 °C. Flowering timing was defined as the emergence of the first visible floral stem formation (bolting), as well as the number of rosette leaves at the first visible stem formation. At least 10 replicates were used for each experiment, and each experiment was repeated three times. Mutant genotypes were compared to the wild type under both control and salt-stressed conditions. Statistical differences were determined using Student's two tailed *t* test, one-way analysis of variance (ANOVA), or two-way ANOVA, where appropriate.

RNA in situ hybridization and histological staining

For RNA in situ hybridization and toluidine blue staining plants were grown on MS agar plates under LD at 22 °C. Meristem (vegetative and inflorescence) and silique samples were harvested, fixed and embedded into wax using an automated tissue processor (Leica ASP200S, Leica, Wetzlar, Deutschland) and embedding system (HistoCore Arcadia, Leica). Sections of 8 µm thickness were prepared using a rotary microtome (Leica RM2255; Leica).

Briefly, for toluidine blue staining slides containing sections were incubated twice in Histoclear solution (Biozym Scientific, Hessisch Oldendorf, Germany) and an ethanol series: 100% EtOH for 2 min, 100% EtOH for 2 min, 95% of EtOH for 1 min, 90% of EtOH for 1 min, 80% of EtOH for 1 min, 60% of EtOH + 0.75% of NaCl for 1 min, 30% EtOH + 0.75% of NaCl for 1 min, 0.75% NaCl for 1 min and PBS for 1 min. Afterwards, the slides were left to dry at 42 °C and then incubated in 0.01% toluidine blue/sodium borate solution for 2 min, briefly washed with water and 80% EtOH. The sections were imaged with the Nikon eclipse E600 microscope using NIS-Elements BR 4.51.00 software. Adobe Photoshop CS5 was used to generate the figures.

RNA in situ hybridizations were performed by processing slides containing sections through the Histoclear and ethanol series. Next, slides were incubated in Proteinase K (Roche, Mannheim, Germany) and *FRIENDLY MITOCHONDRIA* (*FTM)* probes were mixed with hybridization buffer and applied to the slides for overnight hybridization. The *FMT* probes were amplified and cloned into pGEM-T Easy Vector (Promega, Madison, Wisconsin, USA) using the following primers: forward (FMTpGEMFW) 5′-ATGGCTGGGAAG TCGAAC-3′ and reverse (FMTpGEMRV) 5′-TTATTTTTT GGCTTTTTGCTTCTTC-3′, and synthesized with the DIG RNA Labeling Kit (Roche). After the hybridization overnight, slides were washed out and incubated for with 1% blocking reagent (Roche) in 1 × TBS/0.1% Triton X-100. For immunological detection, the Anti-DIG antibody (Roche) solution diluted 1:1,250 in blocking reagent was applied to the slides. For the colorimetric detection, the NBT/BCIP stock solution (Roche) diluted 1:50 in 10% polyvinyl alcohol (PVA) in TNM-50 was applied to the slides. The slides were incubated overnight and sections were imaged as described above.

Transmission electron microscopy (TEM)

Arabidopsis seedlings were grown on MS-agar plates for one week, and were then transferred to either 125 mM NaCl MS-agar plates or MS-agar plates without the addition of NaCl for an additional week. Fixation and embedding of 14-day-old root samples was done according to [51] with the following modifications: Durcupan epoxy resin (Sigma) was used for infiltration, tissue was collected on single slot copper grids (EMS) coated with formvar, and no post-sectioning heavy metal staining was used. Transverse sections were cut ~ 30 µm deep into the columella of the root and subsequently viewed under a Tecnai 12 Transmission Electron Microscope (FEI, USA). At least ten cells from four biological samples each of WT, *fmt*, and *FMT-OE* roots were examined for control experiments, and at least ten cells from three biological samples each of WT, *fmt*, and *FMT-OE* roots were examined for salt-stressed experiments.

Cell quantification and analysis

Using Fiji, individual cells, nuclei, vacuoles, and mitochondria were traced and measured to give the following parameters: area, aspect ratio (AR), number of mitochondria per cell, and centroid XY coordinates of each individual mitochondrion. Mitochondrial coverage was calculated as a percent using the following formula: ((cytoplasmic area–mitochondrial area) × 100), where cytoplasmic area = (cell area–nuclear area–vacuole area), and mitochondrial area is the sum of all the areas of the individual mitochondria within the cell. Mitochondrial clustering was calculated using the Nearest Neighbor Distances (NND) tool in the BioVoxxel toolbox plugin in Fiji (http://imagej.net/BioVoxxel_Toolbox). The NND tool measures the average nearest neighbor ratio (ANN), which is given as:

$$\mathrm{ANN} = \frac{\overline{D}_{\mathrm{O}}}{\overline{D}_{\mathrm{E}}},$$

where $\overline{D}_{\mathrm{O}}$ is the observed mean distance between each feature and its nearest neighbor:

$$\overline{D}_{\mathrm{O}} = \frac{\sum_{i=1}^{n} d_i}{n}$$

and $\overline{D}_{\mathrm{E}}$ is the expected mean distance for the features given in a random pattern:

$$\overline{D}_{\mathrm{E}} = \frac{0.5}{\sqrt{n/A}}.$$

In the above equations, d_i equals the distance between feature i and its nearest neighboring feature, n corresponds to the total number of features, and A is the area of a minimum enclosing rectangle around all features.

The average nearest neighbor z-score for the statistic is calculated as:

$$z = \frac{\overline{D}_{\mathrm{O}} - \overline{D}_{\mathrm{E}}}{\mathrm{SE}},$$

where:

$$\mathrm{SE} = \frac{0.26136}{\sqrt{n/A}}.$$

If the average distance is less than the average of a hypothetical random distribution, the mitochondria are considered clustered. If the average distance is greater than a hypothetical random distribution, the mitochondria are considered dispersed.

Experimental set-up for measuring 3D growth behavior using phytotyping^{4D}

The Phytotyping^{4D} system provides continuous 3D recordings using a light-field camera, which allows the viewer to very accurately measure the growth rate of a plant. In particular, the camera provides both a 2D focus and a depth image simultaneously, allowing for a 3D surface reconstruction of the plant [1, 2]. Furthermore, by employing near-infrared light, Phytotyping^{4D} can continuously and non-invasively record growth over several days during light and dark periods. Arabidopsis plants were grown in 10 cm diameter pots that were filled with soil and watered containing fungicide and boric acid solution. In each pot, four equidistant spots were sown with 10–20 seeds per spot and kept for 3 days covered from light in a cold room (4 °C) for stratification. Next, the plants were grown in 12 h light /12 h dark neutral days in a growth chamber (model E-36L; Percival Scientific Inc., http://www.percival-scientific.com/) with 20 °C during the day and 18 °C in the night and a photosynthetically active radiation of 160 µmol m^{-2} s^{-1} at the plant level. After one week, plants were thinned to one plant per spot and 15 days later the imaging was performed in the same growth chamber with Phytotyping^{4D} for 8 days. To reduce near-infrared light reflection, the soil surface was covered with black plastic-coated quartz sand before imaging. Recordings were analyzed as described in Apelt et al. [1] obtaining non-invasive measurements of growth, RER, and hyponasty with high spatio-temporal resolution.

Behavioral assessments of *Cluh*$^{\pm}$ mice

The Institutional Animal Care and Use Committee of Yale University approved all experiments. Mice were kept under standard laboratory conditions with free access to standard chow food and water except during behavioral testing periods. The generation of *Cluh*$^{\pm}$ mice has been previously described [42]. Animals included in behavioral studies were between 8 weeks of age. A series of behavioral assessments were used to establish the behavioral phenotype of *Cluh*$^{\pm}$ mice, including marble bury, open field, and elevated zero maze. All behavioral testing was done in the light phase.

Marble burying test

The marble-burying test was as described [11] with the following modifications: The test was performed in a static mouse cage containing 24 evenly distributed marbles arranged in a 4 × 6 pattern with alternating blue and white marbles. The marbles were placed on top of 5 cm of mouse bedding.

Open field

The open field apparatus is a square, polyurethane box (35.5 cm × 35.5 cm × 30 cm). The animal was placed in the center of the apparatus. General locomotion parameters (distance traveled, locomotion speed, time mobile) and parameters relating to anxiety (freezing time; time spent, distance traveled and entries into central and periphery zones) were recorded for 10 min. The apparatus was cleaned with 70% ethanol after each animal exposure. ANY-Maze Software (Stoelting Company, Wood Dale, IL) was used to record and analyze the behavioral data.

Elevated zero maze

The elevated zero maze is an elevated (60 cm high) ring-shaped runway (5 cm wide), with 2 equally sized (25% of the runway length) sections closed off by walls (40 cm high) opposite each other. The other two sections are open. The maze is equally illuminated on all four sections. Mice were placed on the center of one of the open sections, facing one of the closed sections, and allowed to explore the maze for 5 min. The apparatus was cleaned with 70% ethanol after each animal exposure. ANY-Maze Software (Stoelting

Company, Wood Dale, IL) was used to record and analyze the behavioral data.

Supplementary Information The online version contains supplementary material available at https://doi.org/10.1007/s00018-022-04382-3.

Acknowledgements This work was supported by grants from the National Institute of Health: AG052005, AG052986, AG051459, DK111178 to T.L.H. Work in the Mueller-Roeber group is supported by the Deutsche Forschungsgemeinschaft (DFG) grant within the Collaborative Research Centre 973 'Priming and Memory of Organismic Responses to Stress' (http://www.sfb973.de). We thank Life Science Editors for editing assistance at earlier version of the manuscript.

Author contributions Conceived and designed study, AR and TLH; performed experiments, AR, FA, and JJO; analyzed results, AR, FA, and JJO; provided essential materials, FK, BMR, EIR and TLH; wrote the manuscript, AR and TLH; edited manuscript, all authors.

Funding This work was supported by Grants from the National Institute of Health: AG052005, AG052986, AG051459, DK111178 to T.L.H. Work in the Mueller-Roeber group is supported by the Deutsche Forschungsgemeinschaft (DFG) grant within the Collaborative Research Centre 973 'Priming and Memory of Organismic Responses to Stress' (http://www.sfb973.de).

Data availability The datasets generated during and/or analyzed during the current study are not publicly available but are available from the corresponding author on reasonable request.

Declarations

Conflict of interest Authors declare no competing interest.

Ethical approval Animal work related to this study was approved by the Yale Institutional Animal Care and Use Committee.

Consent to participate Not applicable.

Consent to publish Not applicable.

References

1. Apelt F, Breuer D, Nikoloski Z, Stitt M, Kragler F (2015) Phytotyping(4D): a light-field imaging system for non-invasive and accurate monitoring of spatio-temporal plant growth. Plant J 82:693–706
2. Apelt F, Breuer D, Olas JJ, Annunziata MG, Flis A, Nikoloski Z, Kragler F, Stitt M (2017) Circadian, carbon, and light control of expansion growth and leaf movement. Plant Physiol 174:1949–1968
3. Aung K, Hu J (2012) Differential roles of Arabidopsis dynamin-related proteins DRP3A, DRP3B, and DRP5B in organelle division. J Integr Plant Biol 54:921–931
4. Bertholet AM, Delerue T, Millet AM, Moulis MF, David C, Daloyau M, Arnaune-Pelloquin L, Davezac N, Mils V, Miquel MC et al (2016) Mitochondrial fusion/fission dynamics in neurodegeneration and neuronal plasticity. Neurobiol Dis 90:3–19
5. Burte F, Carelli V, Chinnery PF, Yu-Wai-Man P (2015) Disturbed mitochondrial dynamics and neurodegenerative disorders. Nat Rev Neurol 11:11–24
6. Busi MV, Maliandi MV, Valdez H, Clemente M, Zabaleta EJ, Araya A, Gomez-Casati DF (2006) Deficiency of *Arabidopsis thaliana* frataxin alters activity of mitochondrial Fe–S proteins and induces oxidative stress. Plant J 48:873–882
7. Chan DC (2006) Mitochondria: dynamic organelles in disease, aging, and development. Cell 125:1241–1252
8. Chen H, Chan DC (2009) Mitochondrial dynamics–fusion, fission, movement, and mitophagy—in neurodegenerative diseases. Hum Mol Genet 18:R169-176
9. Cheng A, Hou Y, Mattson MP (2010) Mitochondria and neuroplasticity. ASN Neuro 2:e00045
10. Cox RT, Spradling AC (2009) Clueless, a conserved Drosophila gene required for mitochondrial subcellular localization, interacts genetically with parkin. Dis Model Mech 2:490–499
11. Deacon RM (2006) Digging and marble burying in mice: simple methods for in vivo identification of biological impacts. Nat Protoc 1:122
12. Deinlein U, Stephan AB, Horie T, Luo W, Xu G, Schroeder JI (2014) Plant salt-tolerance mechanisms. Trends Plant Sci 19:371–379
13. Dinneny JR, Long TA, Wang JY, Jung JW, Mace D, Pointer S, Barron C, Brady SM, Schiefelbein J, Benfey PN (2008) Cell identity mediates the response of Arabidopsis roots to abiotic stress. Science (New York, NY) 320:942–945
14. Duan L, Sebastian J, Dinneny JR (2015) Salt-stress regulation of root system growth and architecture in Arabidopsis seedlings. Methods Mol Biol 1242:105–122
15. El Zawily AM, Schwarzlander M, Finkemeier I, Johnston IG, Benamar A, Cao Y, Gissot C, Meyer AJ, Wilson K, Datla R et al (2014) FRIENDLY regulates mitochondrial distribution, fusion, and quality control in Arabidopsis. Plant Physiol 166:808–828
16. Fait A, Angelovici R, Less H, Ohad I, Urbanczyk-Wochniak E, Fernie AR, Galili G (2006) Arabidopsis seed development and germination is associated with temporally distinct metabolic switches. Plant Physiol 142:839–854
17. Fields SD, Conrad MN, Clarke M (1998) The *S. cerevisiae* CLU1 and D. discoideum cluA genes are functional homologues that influence mitochondrial morphology and distribution. J Cell Sci 111(12):1717–1727
18. Gao J, Schatton D, Martinelli P, Hansen H, Pla-Martin D, Barth E, Becker C, Altmueller J, Frommolt P, Sardiello M et al (2014) CLUH regulates mitochondrial biogenesis by binding mRNAs of nuclear-encoded mitochondrial proteins. J Cell Biol 207:213–223
19. Glaser E, Alikhani N (2010) The organellar peptidasome, PreP: a journey from Arabidopsis to Alzheimer's disease. Biochimica Biophysica Acta Bioenerg 1797:1076–1080
20. Goh LH, Zhou X, Lee MC, Lin S, Wang H, Luo Y, Yang X (2013) Clueless regulates aPKC activity and promotes self-renewal cell fate in Drosophila lgl mutant larval brains. Dev Biol 381:353–364
21. Golpich M, Amini E, Mohamed Z, Azman Ali R, Mohamed Ibrahim N, Ahmadiani A (2017) Mitochondrial dysfunction and biogenesis in neurodegenerative diseases: pathogenesis and treatment. CNS Neurosci Ther 23:5–22
22. Goncalves VF, Andreazza AC, Kennedy JL (2015) Mitochondrial dysfunction in schizophrenia: an evolutionary perspective. Hum Genet 134:13–21
23. Hu Q, Wang G (2016) Mitochondrial dysfunction in Parkinson's disease. Transl Neurodegener 5:14
24. Islam MT (2017) Oxidative stress and mitochondrial dysfunction-linked neurodegenerative disorders. Neurol Res 39:73–82
25. Krols M, van Isterdael G, Asselbergh B, Kremer A, Lippens S, Timmerman V, Janssens S (2016) Mitochondria-associated membranes as hubs for neurodegeneration. Acta Neuropathol 131:505–523
26. Li X, Zhang WS (2008) Salt-avoidance tropism in *Arabidopsis thaliana*. Plant Signal Behav 3:351–353

27. Liberatore KL, Dukowic-Schulze S, Miller ME, Chen C, Kianian SF (2016) The role of mitochondria in plant development and stress tolerance. Free Radic Biol Med 100:238–256
28. Logan DC, Scott I, Tobin AK (2003) The genetic control of plant mitochondrial morphology and dynamics. Plant J 36:500–509
29. Martin M, Colman MJR, Gómez-Casati DF, Lamattina L, Zabaleta EJ (2009) Nitric oxide accumulation is required to protect against iron-mediated oxidative stress in frataxin-deficient Arabidopsis plants. FEBS Lett 583:542–548
30. Mattson MP, Gleichmann M, Cheng A (2008) Mitochondria in neuroplasticity and neurological disorders. Neuron 60:748–766
31. McClung CR (2006) Plant circadian rhythms. Plant Cell 18:792–803
32. Mishra P, Chan DC (2016) Metabolic regulation of mitochondrial dynamics. J Cell Biol 212:379–387
33. Muller NA, Jimenez-Gomez JM (2016) Analysis of circadian leaf movements. Methods Mol Biol 1398:71–79
34. Munns R (2002) Comparative physiology of salt and water stress. Plant, Cell Environ 25:239–250
35. Nunnari J, Suomalainen A (2012) Mitochondria: in sickness and in health. Cell 148:1145–1159
36. Oka N (2016) Pathology of Charcot-Marie-Tooth disease. Brain Nerve 68:21–29
37. Paszkiewicz G, Gualberto JM, Benamar A, Macherel D, Logan DC (2017) Arabidopsis seed mitochondria are bioenergetically active immediately upon imbibition and specialize via biogenesis in preparation for autotrophic growth. Plant Cell 29:109–128
38. Rajasekaran A, Venkatasubramanian G, Berk M, Debnath M (2015) Mitochondrial dysfunction in schizophrenia: pathways, mechanisms and implications. Neurosci Biobehav Rev 48:10–21
39. Robert N, d'Erfurth I, Marmagne A, Erhardt M, Allot M, Boivin K, Gissot L, Monachello D, Michaud M, Duchene AM et al (2012) Voltage-dependent-anion-channels (VDACs) in Arabidopsis have a dual localization in the cell but show a distinct role in mitochondria. Plant Mol Biol 78:431–446
40. Ryu JY, Lee HJ, Seo PJ, Jung JH, Ahn JH, Park CM (2014) The Arabidopsis floral repressor BFT delays flowering by competing with FT for FD binding under high salinity. Mol Plant 7:377–387
41. Ryu JY, Park CM, Seo PJ (2011) The floral repressor BROTHER OF FT AND TFL1 (BFT) modulates flowering initiation under high salinity in Arabidopsis. Mol Cells 32:295–303
42. Schatton D, Pla-Martin D, Marx MC, Hansen H, Mourier A, Nemazanyy I, Pessia A, Zentis P, Corona T, Kondylis V et al (2017) CLUH regulates mitochondrial metabolism by controlling translation and decay of target mRNAs. J Cell Biol 216:675–693
43. Scott I, Tobin AK, Logan DC (2006) BIGYIN, an orthologue of human and yeast FIS1 genes functions in the control of mitochondrial size and number in *Arabidopsis thaliana*. J Exp Bot 57:1275–1280
44. Sen A, Kalvakuri S, Bodmer R, Cox RT (2015) Clueless, a protein required for mitochondrial function, interacts with the PINK1-Parkin complex in Drosophila. Dis Model Mech 8:577–589
45. Shimada TL, Shimada T, Hara-Nishimura I (2010) A rapid and non-destructive screenable marker, FAST, for identifying transformed seeds of *Arabidopsis thaliana*. Plant J 61:519–528
46. Silvertown J, Gordon DM (1989) A framework for plant behavior. Annu Rev Ecol Syst 20:349–366
47. Sun F, Zhang W, Hu H, Li B, Wang Y, Zhao Y, Li K, Liu M, Li X (2008) Salt modulates gravity signaling pathway to regulate growth direction of primary roots in Arabidopsis. Plant Physiol 146:178–188
48. Vallejo AJ, Yanovsky MJ, Botto JF (2010) Germination variation in *Arabidopsis thaliana* accessions under moderate osmotic and salt stresses. Ann Bot 106:833–842
49. Verdin E, Hirschey MD, Finley LW, Haigis MC (2010) Sirtuin regulation of mitochondria: energy production, apoptosis, and signaling. Trends Biochem Sci 35:669–675
50. Wagner S, Behera S, De Bortoli S, Logan DC, Fuchs P, Carraretto L, Teardo E, Cendron L, Nietzel T, Fussl M et al (2015) The EF-hand Ca^{2+} binding protein MICU choreographs mitochondrial Ca^{2+} dynamics in Arabidopsis. Plant Cell 27:3190–3212
51. Wu S, Baskin TI, Gallagher KL (2012) Mechanical fixation techniques for processing and orienting delicate samples, such as the root of *Arabidopsis thaliana*, for light or electron microscopy. Nat Protoc 7:1113–1124
52. Xu XM, Lin H, Maple J, Björkblom B, Alves G, Larsen JP, Møller SG (2010) The Arabidopsis DJ-1a protein confers stress protection through cytosolic SOD activation. J Cell Sci 123:1644–1651
53. Xu XM, Møller SG (2011) The value of Arabidopsis research in understanding human disease states. Curr Opin Biotechnol 22:300–307
54. Zhang X, Hu J (2009) Two small protein families, DYNAMIN-RELATED PROTEIN3 and FISSION1, are required for peroxisome fission in Arabidopsis. Plant J 57:146–159
55. Zhang XC, Hu JP (2008) FISSION1A and FISSION1B proteins mediate the fission of peroxisomes and mitochondria in Arabidopsis. Mol Plant 1:1036–1047
56. Zhu Q, Hulen D, Liu T, Clarke M (1997) The cluA-mutant of Dictyostelium identifies a novel class of proteins required for dispersion of mitochondria. Proc Natl Acad Sci USA 94:7308–7313